ORGANIC CHEMISTRY

Photochemical phosphorus-enabled scaffold remodeling of carboxylic acids

Qiupeng Peng[1], Meemie U. Hwang[1], Ángel Rentería-Gómez[2], Poulami Mukherjee[2], Ryan M. Young[1,3], Yunfan Qiu[1,3], Michael R. Wasielewski[1,3], Osvaldo Gutierrez[2], Karl A. Scheidt[1]*

The excitation of carbonyl compounds by light to generate radical intermediates has historically been restricted to ketones and aldehydes; carboxylic acids have been overlooked because of high energy requirements and low quantum efficiency. A successful activation strategy would necessitate a bathochromic shift in the absorbance profile, an increase in triplet diradical lifetime, and ease of further functionalization. We present a single-flask transformation of carboxylic acids to acyl phosphonates that can access synthetically useful triplet diradicals under visible light or near-ultraviolet irradiation. The use of phosphorus circumvents unproductive Norrish type I processes, promoting selectivity that enables hydrogen-atom transfer reactivity. Use of this strategy promotes the efficient scaffold remodeling of carboxylic acids through various annulation, contraction, and expansion manifolds.

Photochemical processes that harness light to promote bond-forming processes are potentially sustainable and leverage excited-state or radical behavior that departs from traditional reactivity (*1*–*5*). Since Norrish's group (*6*) first reported the photoexcitation of ketones in 1937 and Yang's group (*7*) observed that excited ketones undergo rapid fragmentation in 1958, the photochemistry of carbonyl-containing molecules has progressed substantially (*8*). Various bond-forming processes involving formal [2+2] cycloadditions (*9*, *10*), such as the Paterno-Büchi and DeMayo reactions, have been applied in complex synthesis (*11*–*13*). However, this established photoexcitation strategy faces persistent challenges, such as controlling α-cleavage, which drives the homolysis of carbon-carbon bonds and generates two radical species (Norrish type I). Additionally, hydrogen-atom transfer (HAT) processes may occur, leading to the undesirable formation of enols and alkenes (*14*) (Norrish type II; Fig. 1A). Notably, in comparison to the well-explored photochemistry of ketones (*15*), carboxylic acids and their derivatives have received comparatively less attention because of their absorption edge in the far-ultraviolet range and low quantum efficiency (*16*) (Fig. 1B). Innovative strategies that involve energy transfer for the excitation of carbon-carbon double bonds in unsaturated systems leading to triplet diradicals (*17*–*19*) has emerged as one way to modulate excited carbonyl processes. However, the energy transfer process for the carbonyl group of carboxylic acid derivatives requires substantially higher energy, which impedes this pathway (*20*, *21*). Consequently, there is a captivating opportunity for a strategy to address this challenge with acids, thus potentially opening new activation modes and broadening the use of carboxylic acids (*22*, *23*) and their derivatives (*24*) in photochemical processes.

The main design challenge to engage carboxylic acids directly with light to promote photoexcited reactivity is the lack of reactivity with this functional group. To address this issue, an ideal method for carboxylic acid engagement through modification should involve direct transformation from free carboxylic acids without purification, coupled with a bathochromic shift in the absorbance profile. This shift would enable direct photoexcitation under visible light or near-ultraviolet light without the need for a sensitizer. The activated intermediate could subsequently generate the singlet diradical before intersystem crossing to access the triplet diradical (*25*), which would have a substantially increased lifetime compared with the triplet state of ketones. If successful, this approach would enable control over diradical reactivity, diminish or even eliminate the Norrish type I reaction, and access a new HAT logic encompassing [1,5]-HAT, [1,6]-HAT, and [1,7]-HAT processes while promoting the diradical with broad reactivity (Fig. 1C). Using this strategy, we can efficiently synthesize α-hydroxyl and amino phosphonates, which exhibit a wide variety of biological activity and are abundant in natural products, pharmaceuticals, and agrochemicals (Fig. 1D) (*26*).

The proposed approach uses a phosphorus promoter to realize this process while also establishing a functional handle for subsequent transformations (*27*–*30*). Our phosphorus promoter design enables diverse scaffold remodeling, encompassing annulation, contraction, and expansion. Scaffold remodeling (*31*, *32*), sometimes referred to as skeletal editing, harbors potential for augmenting molecular diversity and complexity, thereby propelling advancements in pharmaceuticals, materials science, and environmental technologies. To illustrate, a variety of carboxylic acids were selected as starting materials and sequentially activated by oxalyl chloride and trimethyl phosphite to generate acyl phosphonates (*33*). Subsequently, photoexcitation to the singlet diradical state followed by intersystem crossing gives access to the triplet excited state. For β– and γ–amino acids, the generated triplet diradical undergoes a selective [1,6]-HAT or [1,7]-HAT process to form [1,5]-diradical or [1,6]-diradical intermediates, respectively, which in turn leads to intramolecular radical-radical coupling and cyclized product formation. In the case of α-proline derivatives, a preference for the [1,5]-HAT process results in a [1,4]-diradical intermediate. This intermediate undergoes homolytic carbon-nitrogen bond cleavage, generating imine- and enol-containing species before O-nucleophilic addition yields the expanded ring product. For pipecolic acids, the same strategy is used to generate imine- and enol-containing intermediates, which form the final ring contraction product via the Mannich reaction because of a preference toward the more stable five-membered ring rather than the unfavored seven-membered ring. (Fig. 2A).

Reaction development

We commenced the optimization process with acylphosphonate **1a** as the model substrate (Fig. 2B). The use of nonpolar solvents such as dichloromethane, toluene, and chlorobenzene facilitated the smooth production of the desired product with high yields and moderate diastereoselectivity (Fig. 2B, entries 1 to 4). Conversely, more polar solvents, for example, dimethylformamide, acetone, and ethyl acetate, yielded only moderate conversion with a correspondingly lower yield (Fig. 2B, entries 5 to 8). By transitioning to a light-emitting diode (LED) light source emitting at 427 nm (Fig. 2B, entry 9), a noteworthy deceleration in the reaction rate was observed. In the subsequent refinement of the reaction conditions, we selected toluene as the solvent, demonstrating its efficacy in the single-flask version for the synthesis of carboxylic acid–derived products. This protocol exhibited robustness at larger scales, as evidenced by the successful generation of the desired product on a 2.4-g scale (66% yield over three steps) without the need for chromatographic purification (Fig. 2B, entry 10). Alteration of the protecting group (Fig. 2B, entries 11 to 13) between Ts (toluenesulfonyl), Ns (naphthalene-2-sulfonyl), Fmoc (fluorenylmethoxycarbonyl), and the bulkier trisyl (2,4,6-triisopropylbenzenesulfonyl) group (71% yield over three steps, 89% average yield for each step) resulted in a subtle enhancement in diastereoselectivity. In addition, we conducted a series of control experiments to confirm the indispensable role of light in the generation of diradical species (Fig. 2C). The

[1]Department of Chemistry, Northwestern University, Evanston, IL 60208, USA. [2]Department of Chemistry, Texas A&M University, College Station, TX 77843, USA. [3]Paula M. Trienens Institute for Sustainability and Energy, Northwestern University, Evanston, IL 60208, USA.
*Corresponding author. Email: scheidt@northwestern.edu

Downloaded from https://www.science.org at University Van Amsterdam on April 13, 2025

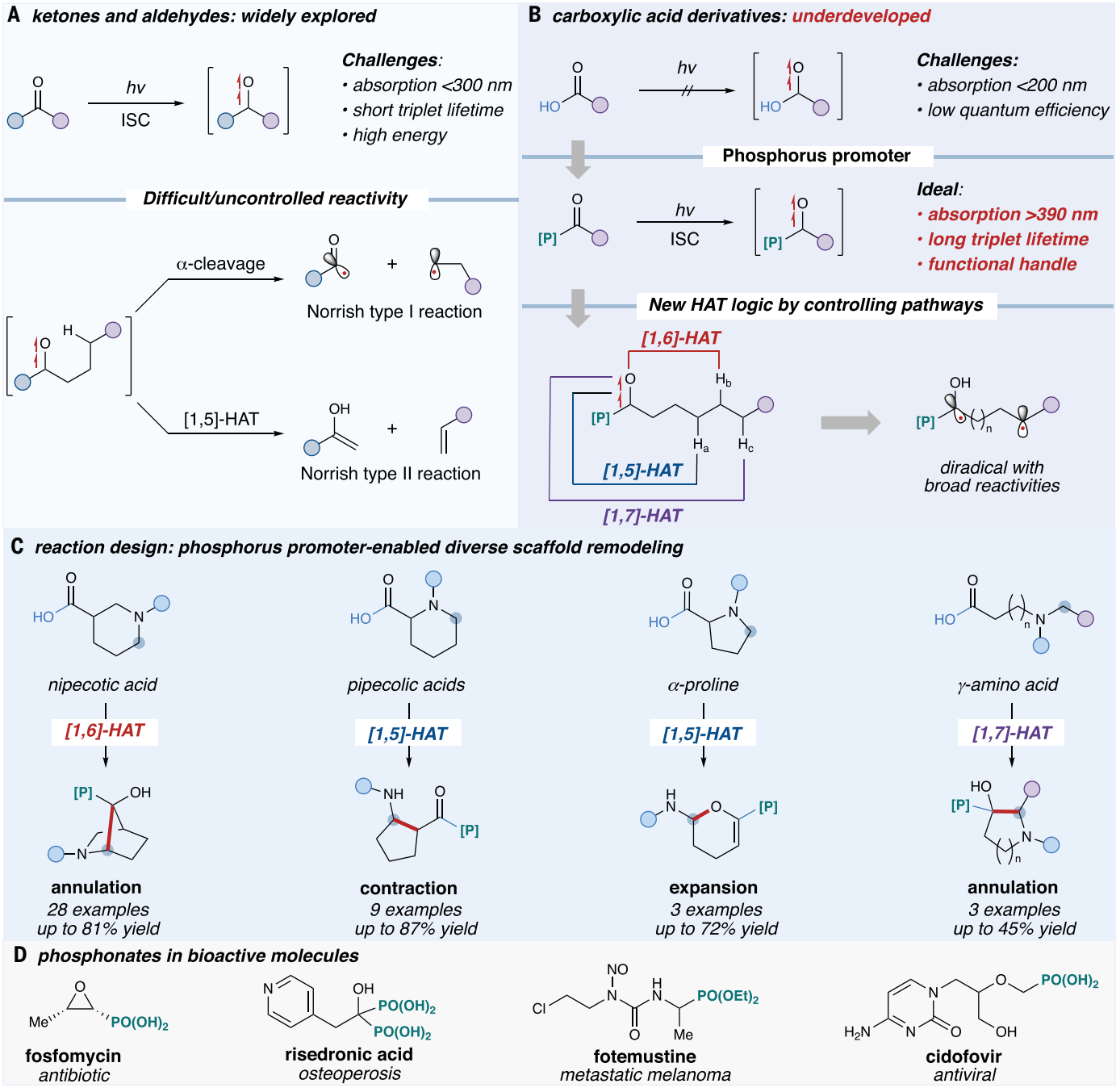

Fig. 1. Carboxylic acid scaffold remodeling concept at visible wavelengths. (**A**) Photoexcitation of ketones and aldehydes. (**B**) The challenges and opportunities for photoexcitation of carboxylic acids. (**C**) The phosphorus promoter–enabled diverse scaffold remodeling of carboxylic acids. (**D**) The α-hydroxyl and amino phosphonates in bioactive molecules.

introduction of radical scavengers such as TEMPO (2,2,6,6-tetramethylpiperidinyloxy) was found to markedly diminish the overall yield, supporting the operation of a single-electron process. In addition, the presence of a triplet quencher, oxygen, resulted in a decreased yield. In a surprising outcome, the addition of 10.0 equivalents of water did not impede the formation of the desired product, yielding a satisfactory outcome.

With the optimized conditions established, we commenced an extended exploration of substrate scope (Fig. 3). When using a variety of phenyl ring substitutions encompassing both electron-withdrawing and electron-donating groups, our methodology consistently yielded the desired products with commendable yields (**2e** to **2j**). Naphthalene and furan-substituted β–amino acids also furnished the corresponding products in 52 and 47% yield, respectively (**2k** and **2l**). The reactivity of linear alkyl-substituted β–amino acid starting materials was investigated under identical conditions, resulting in smooth conversion to pyrrolidines with modest yields (along with other unidentified side products) (**2m** to **2o**). Furthermore, investigations into the propargyl (**2p**) and allylic (**2q**) C–H bond-containing substrates revealed their susceptibility to a [1,6]-HAT process, yielding the targeted products. Notably, the examination

Downloaded from https://www.science.org at University Van Amsterdam on April 13, 2025

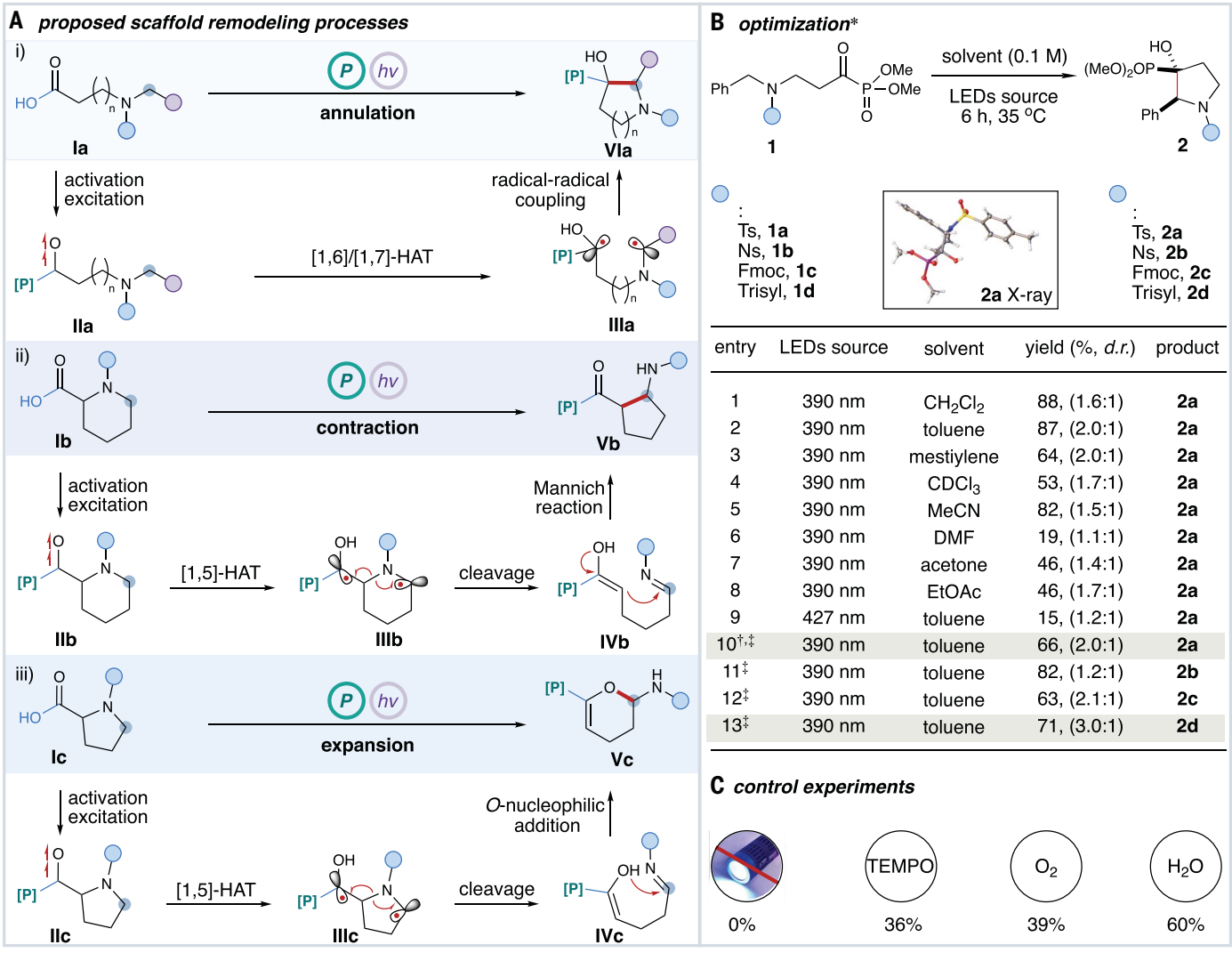

entry	LEDs source	solvent	yield (%, *d.r.*)	product
1	390 nm	CH_2Cl_2	88, (1.6:1)	**2a**
2	390 nm	toluene	87, (2.0:1)	**2a**
3	390 nm	mestiylene	64, (2.0:1)	**2a**
4	390 nm	$CDCl_3$	53, (1.7:1)	**2a**
5	390 nm	MeCN	82, (1.5:1)	**2a**
6	390 nm	DMF	19, (1.1:1)	**2a**
7	390 nm	acetone	46, (1.4:1)	**2a**
8	390 nm	EtOAc	46, (1.7:1)	**2a**
9	427 nm	toluene	15, (1.2:1)	**2a**
10†,‡	390 nm	toluene	66, (2.0:1)	**2a**
11‡	390 nm	toluene	82, (1.2:1)	**2b**
12‡	390 nm	toluene	63, (2.1:1)	**2c**
13‡	390 nm	toluene	71, (3.0:1)	**2d**

Fig. 2. Reaction development. (**A**) The scaffold remodeling mechanisms for β– and γ–amino acids, α-prolines, and pipecolic acids. (**B**) β–amino acid scaffold remodeling reaction optimization table. *Reactions were conducted at 0.10-mmol scale, with acyl phosphonate as starting material; yield was determined by ^{1}H nuclear magnetic resonance (NMR) using 1,3,5-trimethoxybenzene as internal standard; diastereomeric ratios were determined by ^{1}H NMR analysis of unpurified reaction mixtures; and major diastereomer was assigned by x-ray crystallography. †A 10.0-mmol scale reaction yielded **2a** after recrystallization from toluene and dichloromethane (20:1, v/v). ‡Carboxylic acids were used as starting materials. (**C**) Control experiment conditions were as follows: 0.10 mmol, with acyl phosphonate **1d** as starting material; no irradiation; 2.0 equivalents of TEMPO; under oxygen atmosphere; and 10.0 equivalents of water added. $CDCl_3$, deuterated chloroform; DMF, dimethylformamide; d.r., diastereomeric ratio; EtOAc, ethyl acetate; Me, methyl; MeCN, acetonitrile; Ph, phenyl.

of cyclopropane-substituted starting materials yielded exclusively the normal annulation product (**2r**), indicating that five-membered ring formation is faster than cyclopropane ring opening (*34*). Encouragingly, the presence of cyclohexane and tetrahydro-2*H*-pyran moieties did not impede reactivity (**2s** and **2t**). Moreover, the transformations of β–hydroxy acid and β–thio acid derivatives yielded tetrahydrofuran (**2u**) and tetrahydrothiophene (**2v**) scaffolds, respectively. Expanding the applications of this strategy, tranexamic acid and ataluren derivatives were obtained with modest yields (**2w** and **2x**). Salicylic acid derivatives were effectively converted into fused rings (**3a** and **3b**). Notably, cyclic β–amino acids, for example, nipecotic acids (**3c**) and β-proline (**3d**), demonstrated the formation of more intricate [2,2,1] or [2,1,1] bridged rings under the optimized conditions, showcasing the utility of the methodology in synthesizing structurally demanding yet valuable compounds (*35*, *36*). A more challenging [1,7]-HAT process was also successfully realized (**3e** to **3g**), albeit with reduced yields, which presents an intriguing avenue for further investigation, particularly in medicinal chemistry applications. We also demonstrated that α-hydroxyl phosphonates can react with another nucleophile at the ipso position or with an electrophile at the α position under mild conditions in good yields (**6** and **7**, respectively) (*37*, *38*).

Our focus then shifted toward exploring scaffold remodeling of cyclic α–amino acids, guided by the principle that a phosphorus promoter induces a selective [1,5]-HAT process (Fig. 4). This process was strategically used before Mannich reactions or O-nucleophilic addition reactions to achieve ring contraction or expansion. If the nucleophile was introduced before light irradiation, the corresponding amide was formed. However, this amide cannot be converted into the ring contraction product under exposure to the same photochemical conditions. A tetrahydroisoquinoline derivative was successfully transformed into an indene core (**4a**) with a high yield and diastereomeric ratio. Furthermore, piperazine, morpholine, and thiomorpholine

Downloaded from https://www.science.org at University Van Amsterdam on April 13, 2025

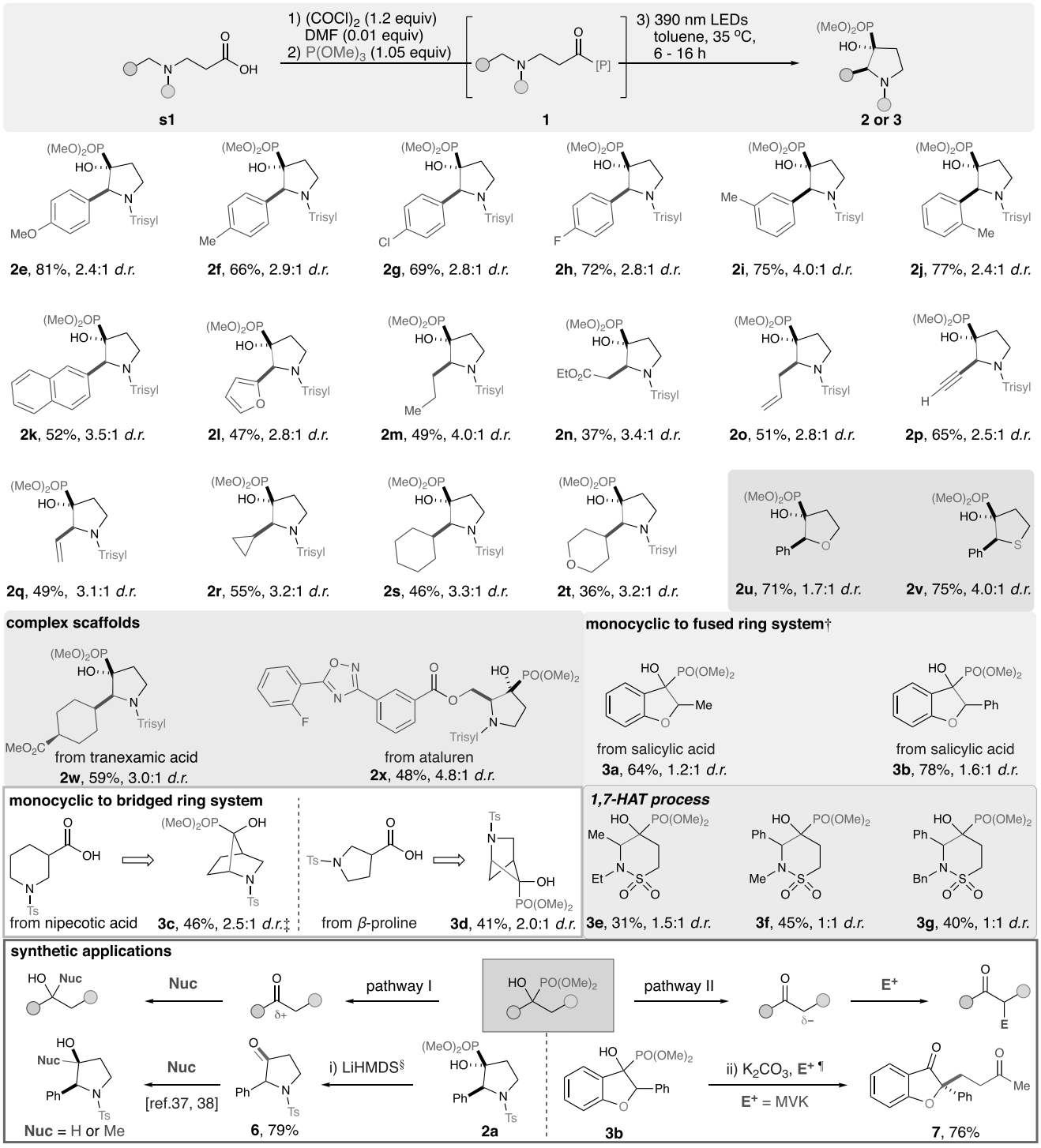

Fig. 3. Substrate scope for β– and γ–amino acid annulation via a [1,6]- or [1,7]-HAT process. *Reactions were conducted at 0.20-mmol scale, with carboxylic acid used as starting material; isolated yields are reported; and diastereomeric ratios were determined by ^{1}H NMR spectroscopic analysis of unpurified reaction mixtures. †456-nm LEDs were used. ‡MeCN was used as solvent. §Reaction conditions were as follows: **2a** (0.10 mmol), LiHMDS [lithium bis(trimethylsilyl)amide, 1.05 equivalents], MeCN (0.1 M), −30°C, 10 min. ¶Reaction conditions were as follows: **3b** (0.10 mmol), K_2CO_3 (3.0 equivalents), MVK (methyl vinyl ketone, 3.0 equivalents), MeCN (0.1 M), 40°C, 6 hours. Et, ethyl.

derivatives underwent ring contraction to furnish 2,3-*cis*-disubstituted pyrroline (**4b**), tetrahydrofuran (**4c**), and tetrahydrothiophene (**4d**), respectively, with moderate to high yields and excellent diastereoselectivity. Introduction of the chiral phosphoric acid-(*R*)-TRIP catalyst [(*R*)-3,3′-bis(2,4,6-triisopropylphenyl)-1,1′-binaphthyl-2,2′-diyl hydrogenphosphate] into the reaction system enabled the synthesis of *cis*-2-amino-1-cyclopentanecarboxylic acid derivatives with excellent enantioselectivity (**4e**). We demonstrated the versatility of this phosphorus functional

Downloaded from https://www.science.org at University Van Amsterdam on April 13, 2025

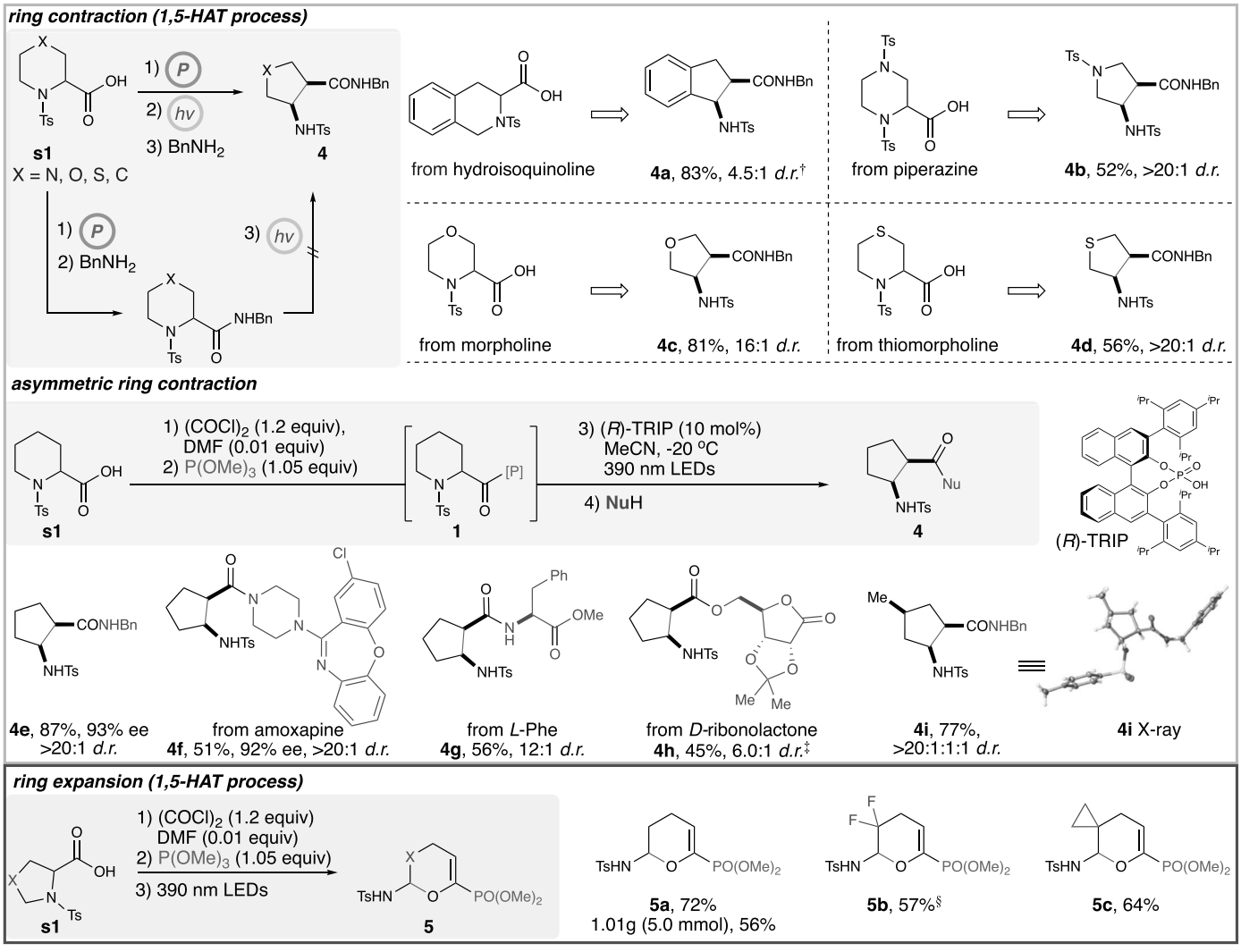

Fig. 4. Substrate scope for cyclo-α–amino acid ring contraction or expansion via a [1,5]-HAT process. *Reactions were conducted at 0.20-mmol scale, with carboxylic acid used as starting material; isolated yields are reported; and diastereomeric ratios were determined by ^{1}H NMR analysis of unpurified reaction mixtures. †0.10 equivalent of diphenyl phosphate was added. ‡1.0 equivalent of 1,8-diazabicyclo[5.4.0]undec-7-ene (DBU) was added when treated with nucleophile. §MeCN was used as solvent. Bn, benzyl; ee, enantiomeric excess; ^{i}Pr, isopropyl.

handle by incorporating different functional nucleophiles in the final step, showcasing its utility in the late-stage functionalization of amoxapine (**4f**), L-Phe (**4g**), and D-ribonolactone (**4h**). Additionally, the transformation of chiral disubstituted piperidine to chiral trisubstituted cyclopentane proceeded with high yield and excellent diastereomeric ratio (**4i**), which was confirmed by x-ray crystallography to establish its absolute configuration (see supplementary materials for additional details). Using α-proline derivatives as starting materials showcased a ring expansion process, furnishing products with good yields (**5a**). The scalability of this chemistry was validated on a 5.0-mmol scale, resulting in gram-scale product with acceptable yields. Difluoride α-proline (**5b**) and cyclopropane α-proline derivatives (**5c**) were compatible, albeit with moderate yields.

Mechanistic experiments and DFT calculations

The acyl phosphonate intermediate **S1-3d**, which we obtained through a single-flask transformation by using a phosphorus promoter, manifests a bathochromic shift in the absorbance profile compared with ketone **S1-3a**, ester **S1-3b**, and free carboxylic acid **S1-3c** (Fig. 5A). This shift enables direct photoexcitation under visible light without the need for a sensitizer. Furthermore, using transient absorption spectroscopy (*39*) revealed that the acyl phosphonate **S1-3d** substantially increases the half-life of triplet diradicals to 785 ± 4 ns, in contrast to the ketone species **S1-3a**, which only possesses a half-life of 195 ± 2 ns (*40*, *41*). It was hypothesized that the diphenylphosphonyl radical is more stable than the dimethoxyphosphonyl radical (*42*, *43*). Consequently, the acyl phosphine oxide prefers the Norrish type I pathway, whereas the acyl phosphonate **S1-3d** exclusively undergoes a HAT process. To further explore the proposed mechanism, we turned to dispersion-corrected density functional theory (DFT) calculations (see supplementary materials for additional details). The first step of the mechanism is presumably the excitation of the acyl phosphonate **1d** under 390-nm-wavelength light irradiation followed by intersystem crossing (ISC) to reach the triplet excited state **1d*** (*44*). To investigate the factors that control selectivity in the HAT step, we explored different potential HAT pathways

Downloaded from https://www.science.org at University Van Amsterdam on April 13, 2025

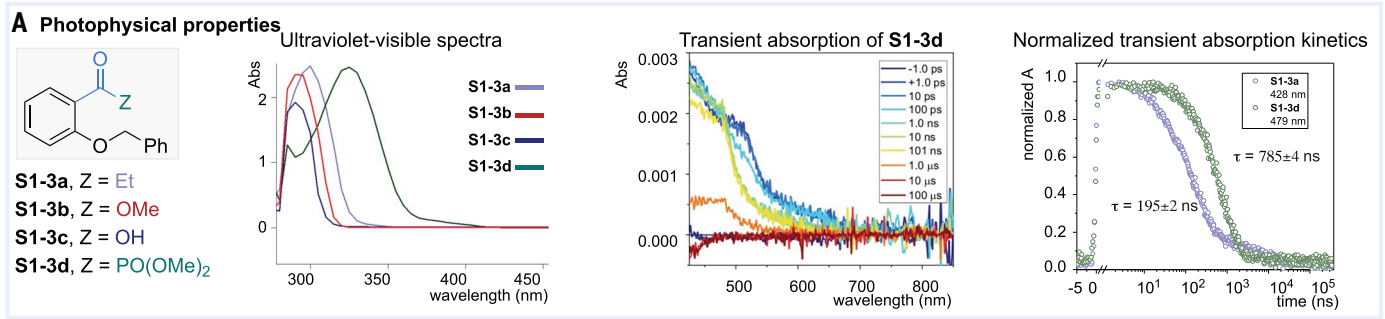

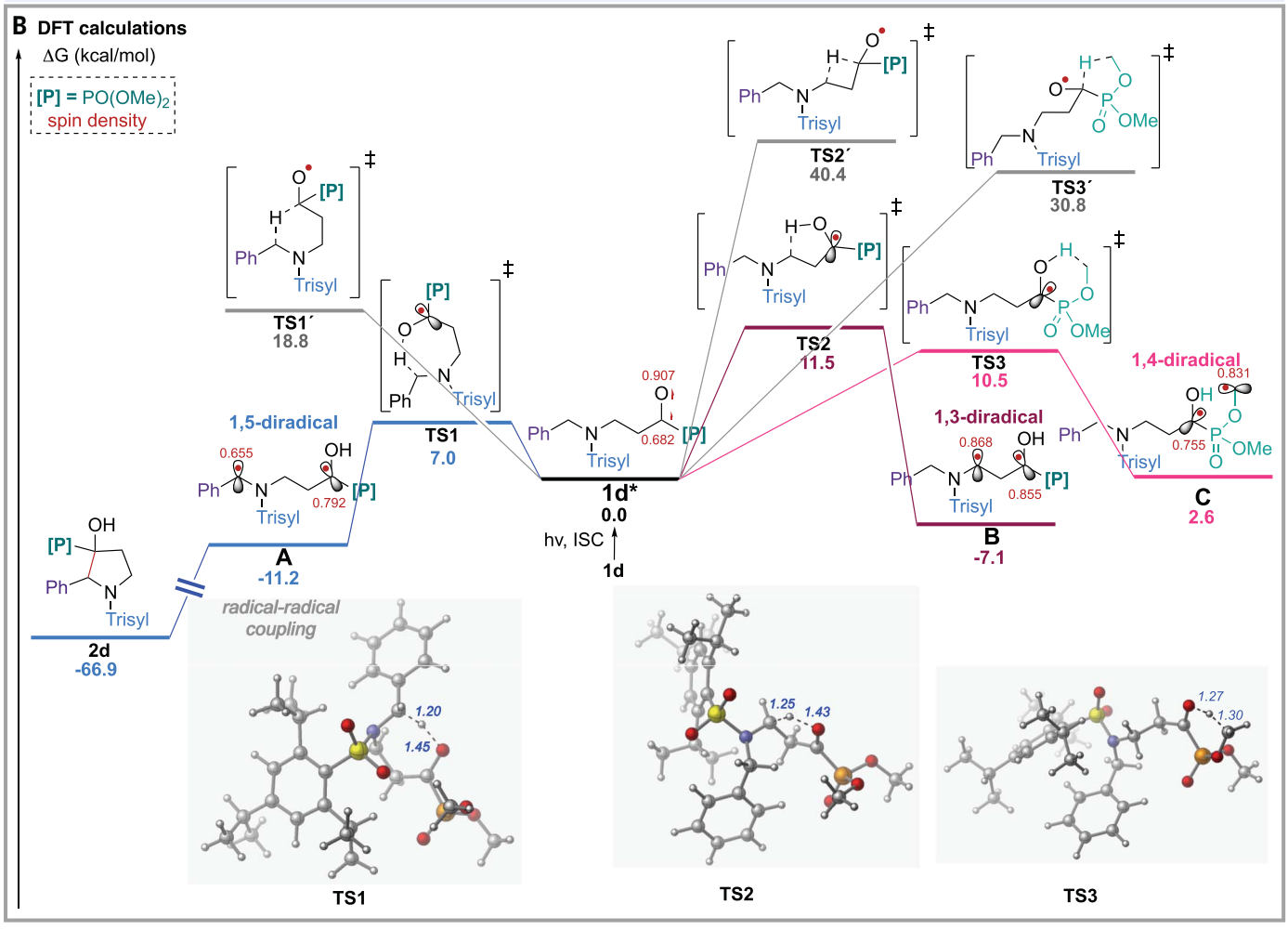

Fig. 5. Mechanism study. (**A**) Photophysical properties. Ultraviolet-visible spectra for 0.1 mM **S1-3a**, **S1-3b**, **S1-3c**, and **S1-3d** in toluene are shown on the left. Transient absorption data for **S1-3d** in degassed toluene excited at 414 nm are shown in the middle. Femtosecond time-resolved absorption spectra of **S1-3a** in toluene for 355-nm excitation in the 0.8-ns to 300-µs temporal window and **S1-3d** in toluene for 414-nm excitation in the 0.8-ps to 300-µs temporal window are shown on the right. (**B**) Proposed mechanism supported by computational studies. Calculated free Gibbs energies (Δ*G*) [CPCM(toluene) uB3LYP-D3/def2-svp] are given in kcal/mol. A, absorbance; Abs, absorbance; τ, half-life.

emanating from intermediate **1d*** (Fig. 5B). Mulliken's spin density analysis of the optimized **1d*** structure showed significant spin density localized at the oxygen atom, consistent with selective O–H bond formation (versus C–H bond formation initiated from the acyl carbon) in the lowest energy HAT step (vide supra). Furthermore, consistent with the observed high regioselectivity, the [1,6]-HAT takes place through a smaller energy barrier via **TS1** (only 7.0 kcal/mol from **1d***) to form the more thermodynamically stable benzylic [1,5]-diradical **A** (11.2 kcal/mol downhill from the excited state intermediate **1d***). In turn, **A** can then undergo irreversible radical-radical C-C coupling to form **2d.** In addition, we explored the alternative [1,4]-HAT and [1,5]-HAT pathways for the O–H bond formation from **1d*** (via **TS2** and **TS3**, respectively). However, the energy barriers were found to be higher (>3 kcal/mol) than those for the [1,6]-HAT process. Although the formation of the **B** radical ([1,3]-HAT) is thermodynamically favored (7.1 kcal/mol downhill from **1d***), the [1,6]-HAT process is both

Downloaded from https://www.science.org at University Van Amsterdam on April 13, 2025

kinetically and thermodynamically favored, presumably because of a less-strained cyclic transition state (**TS1** versus **TS2**; fig. S10) and greater delocalization of the resulting radical intermediate (table S2). Finally, we also considered the possibility of C–H bond formation initiated from the acyl carbon in **1d*** via **TS1′**, but this was ruled out based on the much higher energy barrier for **TS1′** than for **TS1** (18.8 versus 7.0 kcal/mol, respectively).

Conclusions

We have devised a comprehensive strategy that leverages triplet carbonyl chemistry, facilitated by a phosphorus promoter, to achieve diverse scaffold remodeling of carboxylic acids. The multifunctionality of the phosphorus promoter also serves as a functional handle for subsequent transformations. Future investigations include exploring other potential phosphorus-based promoters such as phosphine oxides and developing strategies to enable the promoter to be catalytic in nature.

REFERENCES AND NOTES

1. C. K. Prier, D. A. Rankic, D. W. C. MacMillan, *Chem. Rev.* **113**, 5322–5363 (2013).
2. D. Ravelli, S. Protti, M. Fagnoni, *Chem. Rev.* **116**, 9850–9913 (2016).
3. N. A. Romero, D. A. Nicewicz, *Chem. Rev.* **116**, 10075–10166 (2016).
4. L. Marzo, S. K. Pagire, O. Reiser, B. König, *Angew. Chem. Int. Ed.* **57**, 10034–10072 (2018).
5. P. Melchiorre, *Chem. Rev.* **122**, 1483–1484 (2022).
6. R. G. W. Norrish, C. H. Bamford, *Nature* **140**, 195–196 (1937).
7. N. Yang, D.-D. H. Yang, *J. Am. Chem. Soc.* **80**, 2913–2914 (1958).
8. J. Coyle, H. Carless, *Chem. Soc. Rev.* **1**, 465–480 (1972).
9. J. A. Burkhard, G. Wuitschik, M. Rogers-Evans, K. Müller, E. M. Carreira, *Angew. Chem. Int. Ed.* **49**, 9052–9067 (2010).
10. P. Franceschi, S. Cuadros, G. Goti, L. Dell'Amico, *Angew. Chem. Int. Ed.* **62**, e202217210 (2023).
11. N. Hoffmann, *Chem. Rev.* **108**, 1052–1103 (2008).
12. T. Bach, J. P. Hehn, *Angew. Chem. Int. Ed.* **50**, 1000–1045 (2011).
13. J. M. R. Narayanam, C. R. J. Stephenson, *Chem. Soc. Rev.* **40**, 102–113 (2011).
14. C. Chen, *Org. Biomol. Chem.* **14**, 8641–8647 (2016).
15. J. Jurczyk *et al*., *Science* **373**, 1004–1012 (2021).
16. T. S. Cantrell, *J. Am. Chem. Soc.* **95**, 2714–2715 (1973).
17. C. Brenninger, J. D. Jolliffe, T. Bach, *Angew. Chem. Int. Ed.* **57**, 14338–14349 (2018).
18. F. Strieth-Kalthoff, M. J. James, M. Teders, L. Pitzer, F. Glorius, *Chem. Soc. Rev.* **47**, 7190–7202 (2018).
19. R. Kleinmans *et al*., *Nature* **605**, 477–482 (2022).
20. R. Brimioulle, T. Bach, *Science* **342**, 840–843 (2013).
21. T. R. Blum, Z. D. Miller, D. M. Bates, I. A. Guzei, T. P. Yoon, *Science* **354**, 1391–1395 (2016).
22. Z. Zuo *et al*., *Science* **345**, 437–440 (2014).
23. J. T. Edwards *et al*., *Nature* **545**, 213–218 (2017).
24. A. Fawcett *et al*., *Science* **357**, 283–286 (2017).
25. A. Ruffoni, C. Hampton, M. Simonetti, D. Leonori, *Nature* **610**, 81–86 (2022).
26. K. Moonen, I. Laureyn, C. V. Stevens, *Chem. Rev.* **104**, 6177–6215 (2004).
27. D. A. DiRocco *et al*., *Science* **356**, 426–430 (2017).
28. S. K. Pagire, C. Shu, D. Reich, A. Noble, V. K. Aggarwal, *J. Am. Chem. Soc.* **145**, 18649–18657 (2023).
29. J. Yin *et al*., *Chem* **9**, 1945–1954 (2023).
30. N. B. Bissonnette, N. Bisballe, A. V. Tran, J. A. Rossi-Ashton, D. W. C. MacMillan, *J. Am. Chem. Soc.* **146**, 7942–7949 (2024).
31. Y. Hu, D. Stumpfe, J. Bajorath, *J. Med. Chem.* **60**, 1238–1246 (2017).
32. J. Jurczyk *et al*., *Nat. Synth.* **1**, 352–364 (2022).
33. K.-i. Terauchi, H. Sakurai, *Bull. Chem. Soc. Jpn.* **42**, 821–823 (1969).
34. D. Griller, K. U. Ingold, *Acc. Chem. Res.* **13**, 317–323 (1980).
35. L. Ma, E. H. Sweet, P. G. Schultz, *J. Am. Chem. Soc.* **121**, 10227–10228 (1999).
36. T. Q. Pham *et al*., *J. Med. Chem.* **50**, 3561–3572 (2007).
37. F. A. Davis, T. Ramachandar, H. Liu, *Org. Lett.* **6**, 3393–3395 (2004).
38. A. Hausherr, H. U. Reissig, *Eur. J. Org. Chem.* **2018**, 4071–4080 (2018).
39. S. Aloïse *et al*., *J. Phys. Chem. A* **112**, 224–231 (2008).
40. R. M. Young *et al*., *J. Phys. Chem. A* **117**, 12438–12448 (2013).
41. Y. Wu *et al*., *Angew. Chem. Int. Ed.* **54**, 11971–11977 (2015).
42. G. W. Sluggett, C. Turro, M. W. George, I. V. Koptyug, N. J. Turro, *J. Am. Chem. Soc.* **117**, 5148–5153 (1995).
43. S. Jockusch, N. J. Turro, *J. Am. Chem. Soc.* **120**, 11773–11777 (1998).
44. Q. Peng, A. R. Gogoi, Á. Rentería-Gómez, O. Gutierrez, K. A. Scheidt, *Chem* **9**, 1983–1993 (2023).

ACKNOWLEDGMENTS

We thank J. Zhu (Northwestern) for assistance with the preparation of this manuscript. We also thank S. Shafaie (Northwestern) for assistance with high-resolution mass spectrometry and C. Stern and C. Schull (Northwestern) for their assistance with x-ray crystallography. **Funding:** We thank the National Institute of General Medical Sciences (R35GM136440) for financial support. This work was supported by the US Department of Energy, Office of Science, Office of Basic Energy Sciences, under award no. DE-FG02-99ER14999 (M.R.W.) O.G. acknowledges financial support from the National Institutes of Health (R35GM137797). O.G. also acknowledges the Texas A&M University High Performance Research Computing group (https://hprc.tamu.edu) for computational resources. **Author contributions:** Q.P. and K.A.S. conceived and directed the project. Q.P. and M.U.H. designed, performed, and analyzed the synthetic chemistry experiments. Á.R.-G., P.M., and O.G. designed, performed, and analyzed the computational insight part of the study. R.M.Y. performed and analyzed the transient absorption experiments with samples prepared by Y.Q. Q.P., M.U.H., Á.R.-G., O.G., R.M.Y., and K.A.S. prepared the manuscript. M.R.W., O.G., and K.A.S. acquired funding for the project. **Competing interests:** The authors declare that they have no competing interests. **Data and materials availability:** Cambridge Crystallographic Data Centre (CCDC) nos. 2352355 (**2a**) and 2352354 (**4i**) contain the supplemental crystallographic data for this paper. These data can be obtained free of charge via www.ccdc.cam.ac.uk/data_request/cif, by emailing data_request@ccdc.cam.ac.uk, or by contacting the CCDC. All other data are available in the main text or the supplementary materials. **License information:** Copyright © 2024 the authors, some rights reserved; exclusive licensee American Association for the Advancement of Science. No claim to original US government works. https://www.science.org/about/science-licenses-journal-article-reuse

SUPPLEMENTARY MATERIALS

science.org/doi/10.1126/science.adr0771
Materials and Methods
Supplementary Text
Figs. S1 to S10
Tables S1 to S4
NMR Spectra
References (*45–60*)

Submitted 13 June 2024; accepted 27 August 2024
10.1126/science.adr0771

Downloaded from https://www.science.org at University Van Amsterdam on April 13, 2025